Conformational Preferences of a Synthetic 30mer Peptide from the Interface between the Neck and Stalk Regions of Kinesin[†]

Christian Seeberger,[‡] Eckhard Mandelkow,[§] and Bernd Meyer*,[‡]

*Department of Chemistry, Institute for Organic Chemistry, Martin Luther King Platz 6, D-20146 Hamburg, Germany, and
Max-Planck-Unit for Structural Molecular Biology, Notkestrasse 85, D-22603 Hamburg, Germany*

ABSTRACT: The conformation of a synthetic peptide, consisting of 30 amino acids spanning the neck and hinge regions of rat brain kinesin, was investigated by NMR spectroscopy. The peptide extends from K357 to D386 and has the sequence KSVIQHLEVELNRWRNGEAVPEDEQISAKD. A total of 82 distance range constraints and 23 dihedral angle constraints could be obtained from NOESY and E.COSY spectra, respectively. These were used to calculate 500 structures by applying the REDAC algorithm of the software package DYANA. The first half of the peptide matched the helical structure of the neck determined from an X-ray crystal structure of kinesin. This part normally dimerizes into a coiled-coil by virtue of a leucine zipper interaction, but it is α-helical even in the monomeric state. The second half (not visible in the X-ray structure because of disorder) contains locally defined structure elements (extended chain, helical loop) connected by flexible joints. This is consistent with the "hinge" function postulated for this domain which is important for kinesin's motility and orientation.

The dimeric motor proteins of the kinesin family play a key role in the intracellular transport of vesicles and organelles (*1*−*3*). Furthermore, they are responsible for chromosome transport during cell division (*4, 5*). Kinesins operate along microtubules (MT),[1] which are protein filaments composed of heterodimeric tubulin subunits (*6*). Microtubules are polar structures, their minus-ends are usually anchored near the nucleus, and their plus-ends point toward the cell periphery. Kinesin travels along microtubules from the minus- to the plus-end, thereby converting the chemical energy of ATP into mechanical force (*7, 8*). The heavy chains of kinesin can roughly be divided into three major domains: the head, the stalk, and the tail (*9, 10*). The head carries the ATPase activity and contains the binding sites for ATP and microtubules. The stalk region is an extended helical domain, which contributes to the dimerization of two kinesin heavy chains by forming a coiled coil. The tail is responsible for binding the cargo via light chains (*11, 12*). The overall structure of Kinesin and the sequence of the peptide studied here is shown in Figure 1.

The dimeric nature of kinesin has provided the basis for models of motility which assume a mechanism analogous to walking, i.e., both heads taking alternating steps along a microtubule, with a center-of-mass step size of 8 nm (*7, 8*). This model is currently a matter of debate since there are also monomeric kinesin motors (*13*), but is supported by kinetic evidence (*14*−*16*), the processivity of double-headed but not single-headed kinesin (*17, 18*), and the structure of the kinesin−microtubule rigor complex which shows kinesin heads attached to successive β-tubulin subunits separated by 8 nm (*19, 20*).

The crystal structures of several kinesin motor domains have been determined, both in the monomeric state (*21*−*24*) and in the dimeric state (*25, 26*). The known structures include N-type motors where the motor domain is located at the N-terminus (such as conventional kinesin from human or rat brain) and C-type motors with a C-terminal motor domain (such as Drosophila NCD or yeast KAR3). These motors move in opposite directions, conventional kinesin toward the microtubule plus-end (toward the cell periphery), NCD and KAR3 toward the minus end. The motor domains are quite similar for kinesins from different sources and different putative functions (e.g., vesicle transport or mitosis), but the arrangement of the two monomers in a dimer and the interaction between the motor domains and the neck (the initial part of the stalk) are different (*27, 28*). There are strong indications that the directionality of movement is somehow coded in the interface between the motor domain and sequence elements in the neck or head-neck linker (*29*−*31*). Following the neck helix, kinesin contains a nonhelical hinge region separating the motor unit from the remainder of the stalk. Although it is not part of the core motor domain, this region is an important determinant for motility; perhaps by enabling the head to swivel into a proper orientation for binding (*32*−*34*). Moreover, the neck helix and hinge region may be important for the coordination of the heads because

[1] Abbreviations: MT, microtubules; DMF, dimethylformamide; E.COSY, exclusive correlated spectroscopy; HATU, *O*-(7-azabenzotriazol-1-yl)-*N,N,N′,N′*-tetramethyluroniumhexafluorophosphate; MALDI-TOF, matrix-assisted laser desorption ionization−time-of-flight; NOE, nuclear Overhauser effect; NOESY, NOE spectroscopy; TOCSY, total correlation spectroscopy; PAL, 4-(4-aminomethyl-3,5-dimethoxyphenoxy)-valeric acid; REDAC, redundant dihedral angle constraint; XSA, X-ray structure analysis.
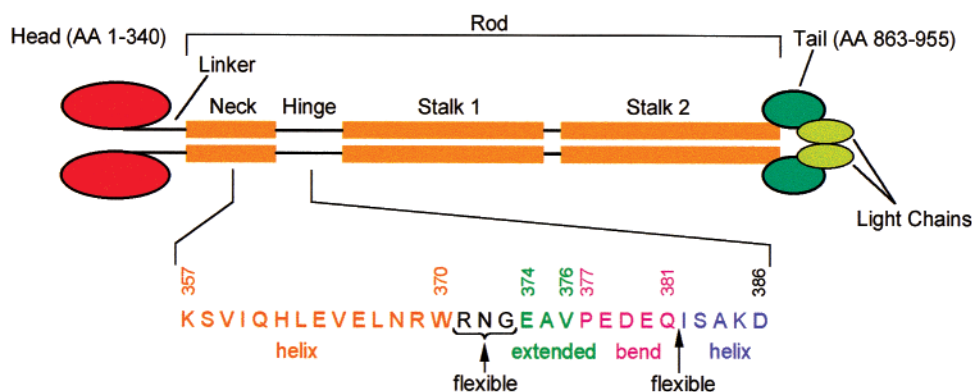
FIGURE 1: Diagram of the kinesin complex, consisting of two heavy and two light chains. Each heavy chain contains an N-terminal motor domain, a central rod domain, and a C-terminal tail domain which binds to the light chain. Downstream of the head domain [residues 1−325 in rat brain kinesin (*23*)] there is a linker region (326−338), the neck helix (339−370, subdivided into segments I and II), and the "hinge" (370−410), followed by the rest of the rod (410−910, interrupted by a kink around 580) and the tail (911−955). The peptide investigated here comprises segment II of the neck helix and the first part of the hinge region (Lys357 to Asp386).

they may have to open up in order to allow one head to advance along the microtubule while the other stays bound (*35, 36*).

The crystal structure of dimeric rat kinesin revealed the head (residues 1−325), the linker (326−338), and neck helix (339−370), but the structure of the hinge remained invisible due to disorder. Because of the importance of the neck-hinge interface for kinesin's motility we have now synthesized a 30-mer peptide, ranging from K357 to D386 that overlaps with 14 residues of the neck known from the X-ray structure and extends by 16 residues into the unknown hinge domain. The structure of the peptide was solved by NMR methods in solution, and in the monomeric state. Despite the differences in conditions between the X-ray and NMR experiments the first half of the NMR structure (corresponding to K357−W370 of rat brain kinesin) was α-helical, similar to segment II of the neck helix in the X-ray structure (*37*), emphasizing that this segment II does not require a coiled-coil dimerization for adopting the helical conformation. The second half shows secondary structure elements (extended chain, coil) joined by flexible linkers that allow the chain to assume a wide range of orientations in space.

MATERIALS AND METHODS

Materials. All protected amino acids, the PAL resin, HATU, DMF, and piperidine were purchased from Perseptive Biosystems. Acetonitrile gradient grade for HPLC was obtained from Fluka. Trifluoroacetic acid was purchased from Sigma. Triisopropyl silane and D_2O were bought from Aldrich. All other chemicals used were obtained from Merck.

Peptide Synthesis. Peptide synthesis was carried out on an automated peptide synthesizer (Perseptive Biosystems, Pioneer), employing Fmoc-protected amino acids and using HATU as activating agent. Two coupling steps per amino acid were performed, using a 3-fold excess of amino acid each. Coupling times were 30 min for the first step and 60 min for the second. The peptide was cleaved from the resin and deprotected in one step using a mixture of trifluoroacetic acid, phenol, ethanedithiol, triisopropylsilane, and water in a volume ratio of 46:1:1:1:1. Two milliliters of this mixture was applied to the resin. After 30 min, the suspension was filtered, and another 2.5 mL of the deprotecting agent was added to the resin. After another 60 min, the suspension was filtered again. The filtrate was lyophilized. The crude product

was dissolved in acetonitrile and lyophilized again. Purification was carried out on reversed phase HPLC, using a gradient of acetonitrile and water with 0.1% trifluoroacetic acid added. Homogeneity of the purified product was ascertained by analytical reversed phase HPLC. After purification 42.9 mg of the peptide were obtained, giving a yield of 24% based on amino groups on the resin.

MALDI-TOF Mass Spectrometry. MALDI-TOF MS was performed on a Biflex III MALDI-TOF Spectrometer from Bruker. For sample preparation, 0.5 μg of peptide were dissolved in 30 μL water. A saturated solution of sinapinic acid in water/acetonitrile (2:1, v:v) was used as matrix. One microliter of each solution was pipetted onto the sample plate and 25 shots were accumulated to a spectrum. The mass spectrum showed the correct molecular mass (measured, *m/z* = 3532.58 (M + H); calculated, M = 3531.94).

NMR Spectroscopy. For preparation of the NMR sample, 5.7 mg of the peptide were dissolved in 600 μL H_2O/D_2O (9:1, v:v). The pH of the sample was set to 3.5 using trifluoroacetic acid. Peptide concentration within the sample was 2.7 mmol/L. All spectra were recorded at 300 K on a Bruker DRX500 NMR spectrometer operating at a frequency of 500 MHz for ^1H. Since the peptide aggregated at higher concentrations, recording of heteronuclear NMR spectra was not possible. The water signal was suppressed using a presaturation pulse during the relaxation delay.

The TOCSY (*38*) spectrum was recorded with a spin lock time of 100.9 ms. Resolution was 512 points in t_1 and 4096 points in t_2. The free induction decay was zero filled to 1024 and 8192 data points in t_1 and t_2 respectively. After multiplication with a phase shifted sine bell the baseline was automatically corrected employing a 5th order polynomial function. The spectral width was set to 10 ppm in both dimensions.

A set of NOESY (*39*) spectra was recorded with mixing times of 25, 50, 75, 100, 150, 300, and 600 ms. The data were recorded with a resolution of 512 points in t_1 and 4096 points in t_2 with a spectral width of 10 ppm. After zero filling to 1024 data points in t_1, a phase shifted sine bell was applied. Automatic baseline correction was carried out as described for the TOCSY spectrum.

An E.COSY (*40*) spectrum was recorded using a resolution of 512 data points in t_1 and 4096 data points in t_2. The

spectrum was zero filled to 1024 data points and 8192 data points, respectively. A phase shifted sine bell function was applied and automatic baseline correction was performed.

Structure Calculation. To obtain structural parameters from the NMR data, the relevant cross-peaks in the NOESY spectra were integrated. NOE build-up curves were plotted and fitted to the double exponential function stated in eq 1 (*41*).

$$A(\tau_m) = V_{max}p_0e^{(-p_2\tau_m)}(1 - e^{(-p_1\tau_m)}) \qquad (1)$$

Equation used to fit the experimental data, where τ_m is the mixing time and V_{max} is the maximum integral volume of the cross-peak. The parameters p_0 and p_1 of the build-up curve were used to calculate the cross relaxation rate σ_0 at $\tau_{mix} = 0$, according to eq 2.

$$\sigma_0 = p_0p_1V_{max} \qquad (2)$$

The inter atomic distance r_{ij} was calculated using the cross relaxation rate and the distance between the two amide protons at the C-terminus of the peptide as a reference (σ_{ref}, r_{ref}) with a value of 1.732 Å. Using eq 3, distances could be calculated from cross relaxation rates.

$$r_{ij} = r_{ref}(\sigma_{ref}/\sigma_{ij})^{1/6} \qquad (3)$$

In cases where build-up curves could not be measured a modified version of eq 3, eq 4 was used to calculate distances out of the values of the integrals A_{ref} and A_{ij}. To negate the effects of spin diffusion the integrals were measured in a spectrum with comparatively short mixing time (100 ms).

$$r_{ij} = r_{ref}(A_{ref}/A_{ij})^{1/6} \qquad (4)$$

The $^3J_{NH-H\alpha}$ coupling constants were determined using the fitting algorithm of Aurelia. The upper and lower anti phase doublets of each cross-peak were fitted to a Lorentzian function and the average of both values was taken. Coupling constants in the E.COSY spectrum were converted to dihedral angles using the Karplus equation given in eq 5.

$$^3J = 6.7\cos^2\theta - 1.3\cos\theta + 1.5 \qquad (5)$$

Only the negative angles closest to the value of $-57°$ (the optimum value for α-helices) were used. The only exception was G373 (cf. text). Using the software package Dyana, 500 structures were calculated from the constraints. Three Redac cycles were carried out, containing 150, 400, and 800 steps with an angle cut off value of 0.4 Å^2 for the first cycle.

RESULTS

Peptide Synthesis. Synthesis of the peptide was carried out using an automated solid-phase peptide synthesizer. A PAL resin which leaves the C-terminus amidated was used and the N-terminus was acetylated at the end of the synthesis. After cleaving, deprotecting, and RP-HPLC, the total yield of peptide was 24%. The MALDI-TOF spectrum of the peptide showed an isotope resolved peak at $m/z = 3532.58$ (M + H) compared to the calculated average isotopic mass of 3531.94 g/mol. Homogeneity of the product was confirmed using analytical reversed phase HPLC.

Table 1: Chemical Shifts for Protons of the Synthetic Peptide[a]

	NH	Hα	Hβ	Hβ'	other
Lys 357	8.237	4.214	1.683	1.752	Hγ, 1.391[b]; Hδ, 1.615[b]
Ser 358	8.311	4.409	3.794[b]		
Val 359	8.077	4.028	2.016		Hγ, 0.854[b]
Ile 360	8.057	3.990	1.752		Hγ1, 1.117; Hγ1', 1.401; H2, Hδ, 0.756[b]
Gln 361	8.292	4.184	1.889	1.937	Hγ, 2.260; Hγ', 2.277
His 362	8.449	4.585	3.139	3.207	H2, 8.557; H4, 7.236
Leu 363	8.236	4.223	1.606[b]		Hγ, 1.508; Hδ1, 0.795; Hδ2, 0.844
Glu 364	8.333	4.263	1.967	2.016	Hγ, 2.387; Hγ', 2.426
Val 365	8.005	3.960	2.006		Hγ1, 0.843; Hγ2, 0.882
Glu 366	8.209	4.253	1.938	1.996	Hγ, 2.337[b]
Leu 367	8.189	4.214	1.576[b]		Hγ, 1.498; Hδ1, 0.785; Hδ2, 0.834
Asn 368	8.249	4.546	2.680[b]		
Arg 369	8.013	4.135	1.576[b]		Hγ, 1.332[b]; Hδ, 2.983[b]
Trp 370	8.023	4.633	3.139	3.217	
Arg 371	7.958	4.135	1.586	1.693	Hγ, 1.411[b]; Hδ, 3.061[b]
Asn 372	8.234	4.624	2.797	2.875	
Gly 373	8.256	3.823			
		3.931			
Glu 374	7.905	4.302	1.889	2.026	Hγ, 2.358[b]
Ala 375	8.222	4.194	1.222		
Val 376	7.970	4.272	1.967		Hγ1, 0.814; Hγ2, 0.854
Pro 377	-	4.311	2.212[b]		Hγ, 1.810; Hγ', 1.947; Hδ, 3.534; Hδ', 3.541
Glu 378	8.383	4.184	1.948	2.007	Hγ, 2.427[b]
Asp 379	8.415	4.594	2.857[b]		
Glu 380	8.150	4.301	1.889	2.074	Hγ, 2.378[b]
Gln 381	8.167	4.253	1.939	2.026	Hγ, 2.227[b]
Ile 382	8.078	4.106	1.811		Hγ1, 1.129; Hγ1', 1.399; Hγ2, Hδ, 0.845[b]
Ser 383	8.233	4.379	3.803[b]		
Ala 384	8.255	4.252	1.342		
Lys 385	8.155	4.204	1.702	1.772	Hγ, 1.371[b]; Hδ, 1.614[b]
Asp 386	8.244	4.507	2.680[b]		

[a] Assignment was achieved using TOCSY and NOESY spectra. All spectra were recorded at 300 K in a mixture of H$_2$O/D$_2$O (9/1 vol/vol). The pH was set to 3.5 using trifluoroacetic acid. Peptide concentration was 2.7 mmol/L. Spin lock time for the TOCSY spectrum and mixing time for the NOESY spectrum were both 100 ms. The signal of the methyl protons of Ala375 was used for calibration of the spectra, a shift of 1.222 ppm was assigned to this signal. [b] Signals of the diastereotopic protons were not dispersed.

Peptide Solubility. During sample preparation for the NMR experiments the peptide showed a strong tendency to aggregate at concentrations over 3 mmol/L by forming a gel. Therefore, the NMR experiments were run at 2.7 mM concentration. For this reason heteronuclear NMR spectra could not be recorded. To obtain information about the oligomerization state of the peptide, independent size exclusion chromatography experiments were carried out (data not shown) with the sample applied in high concentrations. Under these conditions, two different forms of the peptide, i.e., the monomeric form and the di- or trimeric form, could be seen. However, because of the lower concentration of the NMR sample the monomeric form was assumed to be the predominant one under the conditions within the NMR sample. Also, there were no NOE contacts between the side chains of Val 359 and Ile 360 nor of Leu 363 and Glu 364, which should show up if the peptide would form a coiled coil dimer. This together proves that the peptide at NMR concentration is in a monomeric state.

NMR Spectroscopy. The ^{1}H NMR assignments (Table 1) were performed using TOCSY (Figure 2) and NOESY spectra employing the sequential NH$_i$-Hα_{i-1} and NH$_i$-Hβ_{i-1}
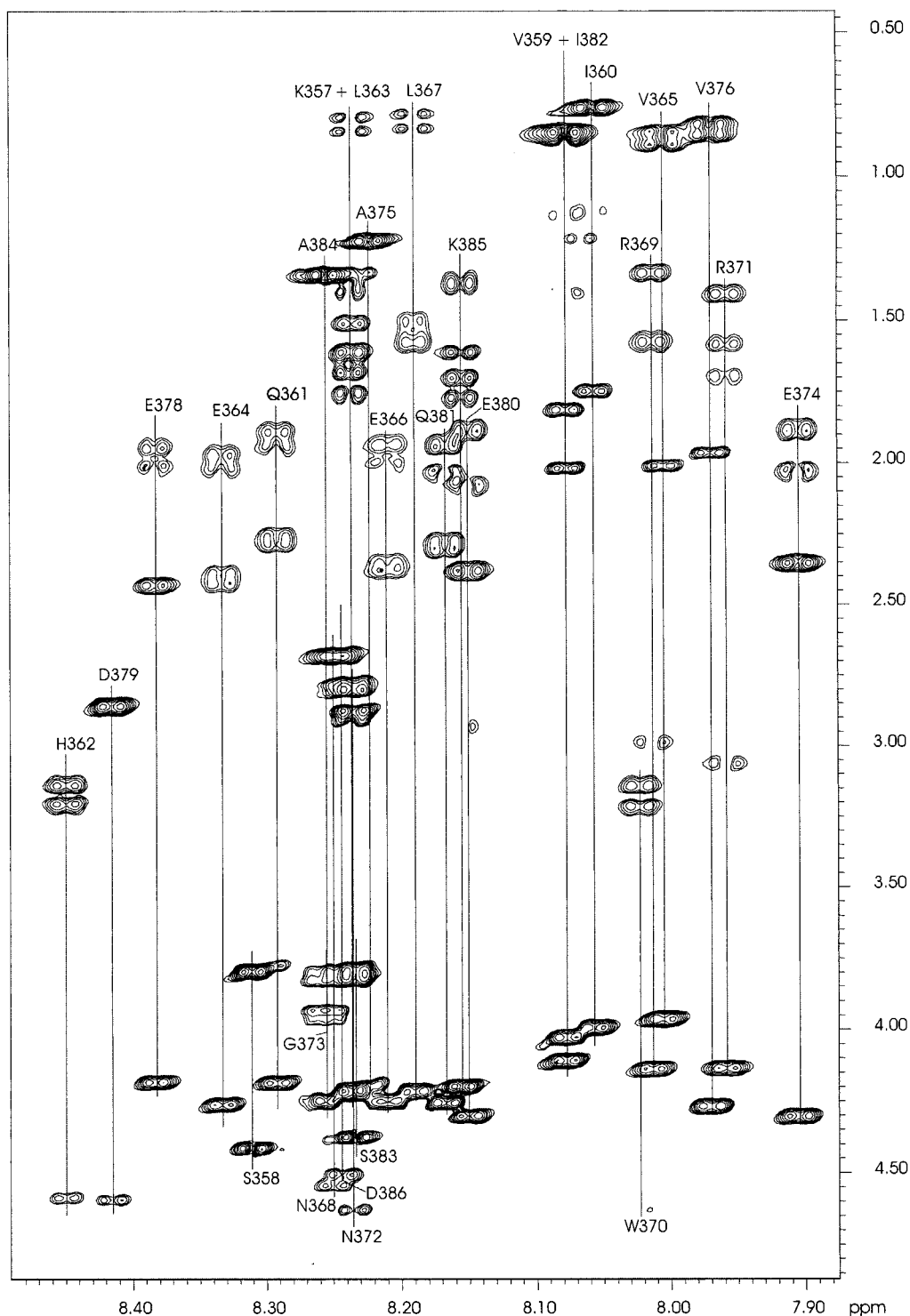
FIGURE 2: NH region of the TOCSY spectrum of the peptide with labeled traces. A total of 2.7 mmol/L peptide concentration in H_2O/D_2O at 300 K and pH 3.5. Assignment of the traces was carried out using sequential NOE contacts.

NOEs (42). The chemical shifts of the NH protons of the residues are dispersed over a range of 0.5 ppm. In the palindromic sequence LEVEL (residues 363−367) the glutamate residues exhibit chemical shifts of their amide protons that differ by 0.12 ppm indicating an ordered region within the peptide. In the sequence, NRWRN (residues 368−372) the two arginines do not show a similar effect. The shifts of the amide protons for these differ only by 0.05 ppm. This is evidence for the increased flexibility within this interval.

Inter proton distances were derived from NOE build-up curves, which were measured using a set of NOESY spectra recorded with seven different mixing times. In case of insufficient data for a build-up curve, the intensity of the corresponding cross-peak was compared to the intensity of a reference peak within the NOESY spectrum recorded with 100 ms mixing time. In both cases, the cross-peak of the C-terminal amide protons was used as reference. A total of 39 distance restraints could be calculated using cross relaxation rates derived from the slope of the NOE build-up
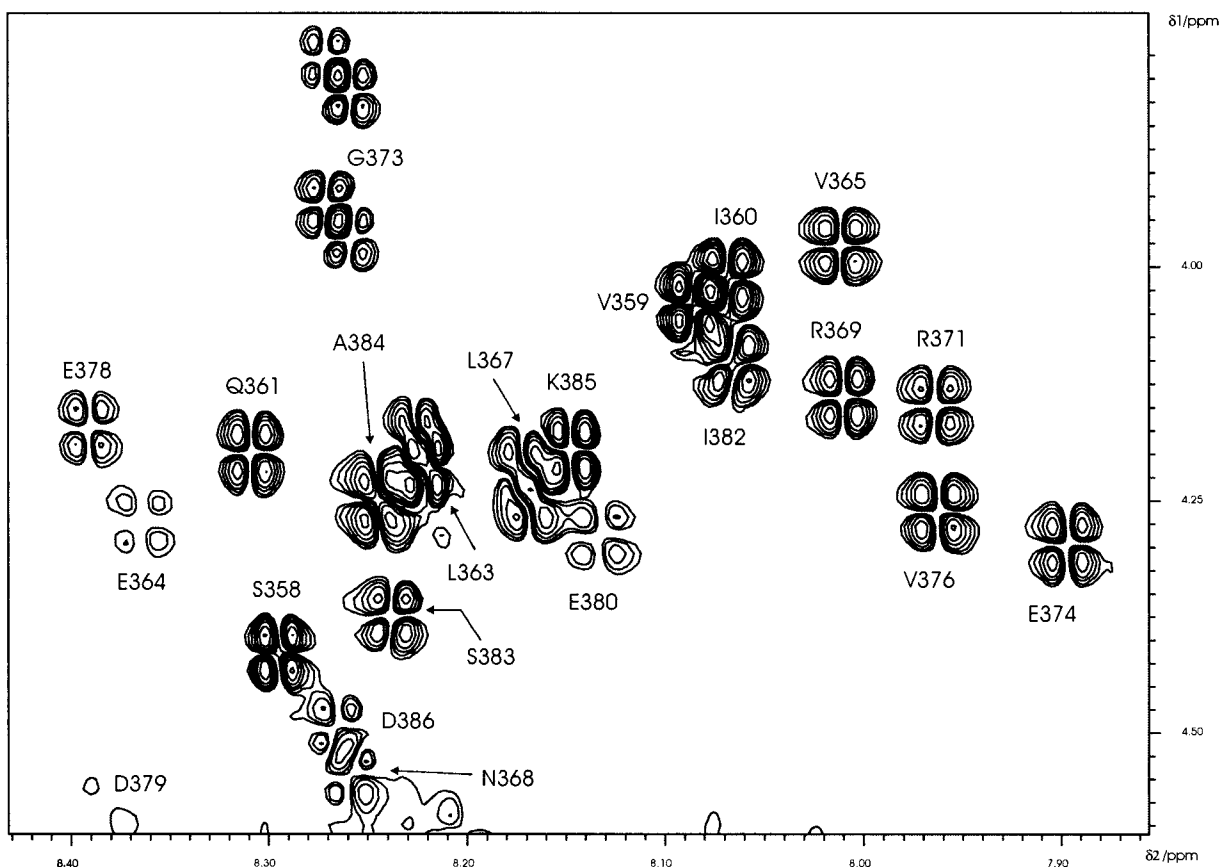
FIGURE 3: Part of the E.COSY spectrum, showing cross-peaks between NH- and Hα-protons. Coupling constants were extracted using a line shape analysis. A total of 2.7 mmol/L peptide concentration in H_2O/D_2O at 300 K and pH 3.5.

curves at mixing time $\tau_m = 0$. A further 37 distance restraints were obtained from analysis of the cross-peak intensities at 100 ms mixing time because for these peaks buildup curves could not be obtained due to overlap and/or low intensity. Constraints for the ϕ-angles could be calculated from NH−Hα coupling constants, which were obtained from an E.COSY (Figure 3) spectrum. Coupling constants and hence dihedral angle constraints were obtained for 23 amino acids.

Structure Calculation. Structure calculation was carried out using the REDAC strategy implemented in the software DYANA (*43*). Since stereospecific assignment of geminal protons was not possible, pseudo atoms were used to represent methylene and methyl groups. Upper and lower limits for inter proton distances were set according to the values derived from NOE build-up curves. To account for inaccuracies of the NMR data the calculated distances were converted to distance ranges. Depending on the overall quality of the build-up curve fitted to the data points, ranges from ±0.2 to ±0.5 Å were added to the calculated distance, giving intervals of 0.4−1.0 Å, respectively. For NOE contacts in the 100 ms spectrum with no corresponding build-up curve, the ranges were classified as short (1.8−2.7 Å), medium (1.8−3.4 Å), and long (1.8−5.0 Å). Since no NOEs were found between G373 and N372 the corresponding distances were set from 5.0 to 10.0 Å. The final distance matrix held 82 lower and upper limits (Table 2). Most of the constraints resulted from sequential (i to $i + 1$) NOEs; however, in the first half of the peptide three weak NOEs between nonadjacent amino acids could be observed. These could be seen between the β-protons of Asn368 and the α-proton of Val365, between the NH−proton of His 362

and the α-proton of Val359 and between the NH−proton of Glu364 and the α-proton of Ile360. These contacts indicate a helical conformation in this interval, albeit the helix should be somewhat flexible since ideal α-helices show more and stronger i to $i + 4$ or i to $i + 3$ NOE contacts.

Constraints for ϕ-angles were calculated using a Karplus equation parametrized for peptides (*44*). Since an α-helical conformation of the peptide was estimated, only the solutions closer to the optimum value of −57° were taken into account. The only exception is G373. Here, both coupling constants NH−Hα and NH−Hα' could be measured and proved to be nearly identical. Therefore, a ϕ-angle of −165° was used in the calculation because this value corresponded best to the symmetrical alignment of the two α-protons. The calculated angles were given a tolerance of ±15°. Since the coupling constants for H362, L363, and D379 could, due to overlap, not be determined with a high precision, here, the tolerance level was expanded to ±25°. All ϕ-angles not otherwise restricted were set to −180° to 0°. Table 3 shows the constraint ranges for the dihedral angles used. The distribution of sequential distance constraints and constraints for ϕ-angles is shown in Figure 4.

The quality of the calculated structures was assessed using the values of their target function. The target function is a measure for the consistency of a structure with the applied constraints; the lower its value, the better the match between structure and constraints. No energy terms are taken into account for calculation of the target function. Of the 500 calculated structures, 433 had a target function value of less than 1 and were chosen for further evaluation. The distribution of selected values for ϕ- and ψ-angles among these 433

Table 2: Distance Ranges Used in the Structure Calculation[a]

atoms		lower limit	upper limit	atoms		lower limit	upper limit
368 Asn QB	367 Leu QD1	1.8	5.00	362 His HN	361 Gln HA	2.88	3.28
368 Asn QB	367 Leu QD2	1.8	5.00	379 Asp HN	378 Glu HA	2.9	3.30
368 Asn QB	365 Val HA	1.8	5.00	378 Glu HN	377 Pro HA	2.69	3.09
376 Val HA	377 Pro QG	1.8	5.00	364 Glu HN	363 Leu HA	2.79	3.19
376 Val HA	377 Pro QD	1.8	5.00	361 Gln HN	360 Ile HA	2.79	3.6
385 Lys HN	384 Ala QB	1.8	5.00	366 Glu HN	365 Val HA	2.52	2.92
362 His HN	361 Gln QB	1.8	5.00	372 Asn HN	371 Arg HA	2.76	3.16
362 His HN	359 Val HA	1.8	5.00	368 Asn HN	367 Leu HA	2.54	3.8
364 Glu HN	360 Ile HA	1.8	5.00	384 Ala HN	383 Ser HA	3.57	3.97
364 Glu HN	363 Leu QD1	1.8	5.00	382 Ile HN	381 Gln HA	2.88	3.48
364 Glu HN	363 Leu QD2	1.8	5.00	360 Ile HN	359 Val HA	2.88	3.48
358 Ser QB	359 Val QG1	1.8	5.00	365 Val HN	364 Glu HA	2.84	3.24
358 Ser QB	359 Val QG2	1.8	5.00	376 Val HN	375 Ala HA	2.65	3.05
381 Gln HN	380 Glu HA	1.8	5.00	374 Glu HN	373 Gly QA	3.14	4.14
385 Lys HN	384 Ala HA	1.8	5.00	383 Ser HN	382 Ile HA	2.46	3.66
359 Val HN	358 Ser HA	1.8	3.40	376 Val HN	375 Ala QB	4.13	4.73
361 Gln HN	360 Ile HB	1.8	5.00	369 Arg HN	368 Asn QB	3.53	4.13
378 Glu HN	377 Pro QG	1.8	5.00	380 Glu HN	379 Asp QB	4.45	5.00
369 Arg HN	369 Arg QD	1.8	5.00	365 Val HN	365 Val HA	2.92	3.52
382 Ile HN	382 Ile HA	1.8	3.40	370 Trp HN	369 Arg HA	2.6	3.00
376 Val HN	376 Val HA	1.8	3.40	361 Gln HN	361 Gln HA	1.8	5.00
372 Asn HN	372 Asn QB	1.8	3.40	374 Glu HN	374 Glu HA	2.7	4.35
375 Ala HN	374 Glu HA	1.8	2.70	375 Ala HN	375 Ala QB	3.57	3.97
361 Gln HN	360 Ile QD1	1.8	3.40	369 Arg HN	369 Arg QB	2.81	3.31
361 Gln HN	360 Ile QG2	1.8	3.40	360 Ile HN	360 Ile HB	3.07	3.67
366 Glu HN	366 Glu QG	1.8	3.40	382 Ile HN	382 Ile HB	3.07	3.87
371 Arg HN	371 Arg QG	1.8	3.40	361 Gln HN	361 Gln QB	3.17	3.77
375 Ala HN	375 Ala HA	1.8	3.40	366 Glu HN	366 Glu QB	2.76	3.36
359 Val HN	358 Ser QB	1.8	5.00	364 Glu HN	364 Glu QB	2.78	3.58
365 Val HN	364 Glu QG	1.8	5.00	376 Val HN	376 Val HB	2.84	3.64
371 Arg HN	370 Trp QB	1.8	5.00	365 Val HN	365 Val HB	2.84	3.24
361 Gln HN	361 Gln QG	1.8	5.00	359 Val HN	359 Val HB	3.17	3.77
378 Glu HN	377 Pro QG	1.8	5.00	379 Asp HN	379 Asp QB	3.45	4.05
364 Glu HN	365 Val HN	1.8	3.40	370 Trp HN	370 Trp QB	3.06	3.46
362 His HN	361 Gln HN	1.8	3.40	362 His HN	362 His QB	3.31	3.91
379 Asp HN	378 Glu HN	1.8	3.40	369 Arg HN	369 Arg QG	3.47	3.87
361 Gln HN	360 Ile HN	1.8	5.00	374 Glu HN	374 Glu QG	4.05	4.45
362 His HN	363 Leu HN	1.8	3.40	364 Glu HN	364 Glu QG	3.77	4.37
358 Ser HN	359 Val HN	1.8	3.40	378 Glu HN	378 Glu QG	4.29	4.69
368 Asn HN	369 Arg HN	1.8	3.40				
372 Asn HN	371 Arg HN	1.8	3.40				
372 Asn HA	373 Gly QA	3.9	10.00				
372 Asn QB	373 Gly QA	5	10.00				

[a] Distance ranges were calculated using either NOE build-up curves (right half of table) or comparison with a reference peak at 100 ms mixing time (left half of table). Pseudo atoms representing diastereotopic protons of methyl and methylene groups are marked with Q.

Table 3: Constraints for ϕ-Angles Used in Structure Calculation[a]

amino acid	ϕ	amino acid	ϕ
Ser 358	−82	Asn 372	−78
Val 359	−88	Gly 373	−162
Ile 360	−87	Glu 374	−88
Gln 361	−82	Val 376	−91
His 362	−82	Glu 378	−74
Leu 363	−78	Asp 379	−87
Glu 364	−85	Glu 380	−86
Val 365	−88	Ile 382	−88
Leu 367	−78	Ser 383	−80
Asn 368	−80	Ala 384	−73
Arg 369	−81	Lys 385	−81
Arg 371	−86		

[a] Torsional angles were derived from ^3J-NH−Hα coupling constants. For structure calculation a tolerance level of ±15° was applied to all values except for His362, Leu363, and Asp379 where a greater tolerance level of ±25° was allowed since the corresponding coupling constants could only be measured less accurately.

FIGURE 4: Distribution of NMR-derived constraints over the peptide sequence. The bold bars represent distances between 1.8 and 3.4 Å, thin bars represent distances between 1.8 and 5.0 Å. The ϕ-angles of residues marked with asterisks were constrained. Noteworthy are the weak medium range NOEs in the first half of the peptide. These are characteristic for helices, while being to weak for an ideal α-helix.

For Q361, R369, and I382 the distribution is broader and covers only 40−60% of the conformers. The plots for all other constrained ϕ-angles show quite broad distributions. As expected, the ψ-angles show more flexibility and their

structures is shown in Figure 5. Very narrow distributions that encompass 70−90% of the 433 structures appear in the segments S358−E364 and V376−D379, as well as for N368.
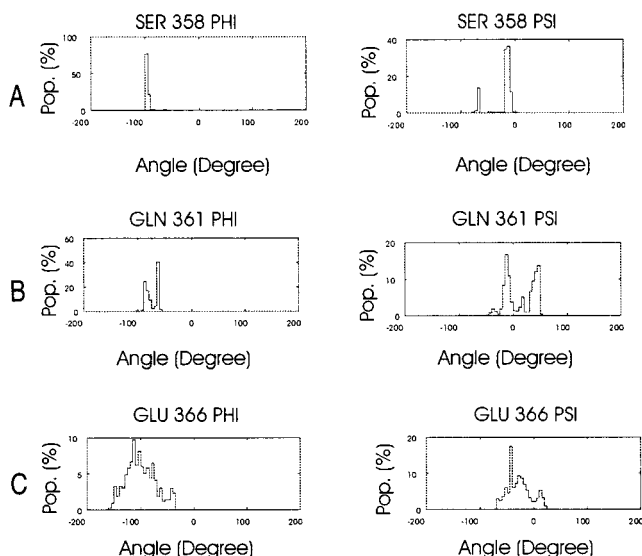
FIGURE 5: Population of dihedral angles in 433 calculated structures. Constraints were applied to 23 out of 30 ϕ-angles. (A) An example of a narrow distribution of ϕ-angles as seen in the intervals S358-E364, V376-D379 and for N368. (B) Example of a broader distribution with a lower population maximum which appear for Q361, R369, and I382. (C) Population of an unconstrained ϕ-angle. The ϕ-angles for K357, E364, W370, N372, A375, P377, and Q381 were unconstrained for structure calculation.
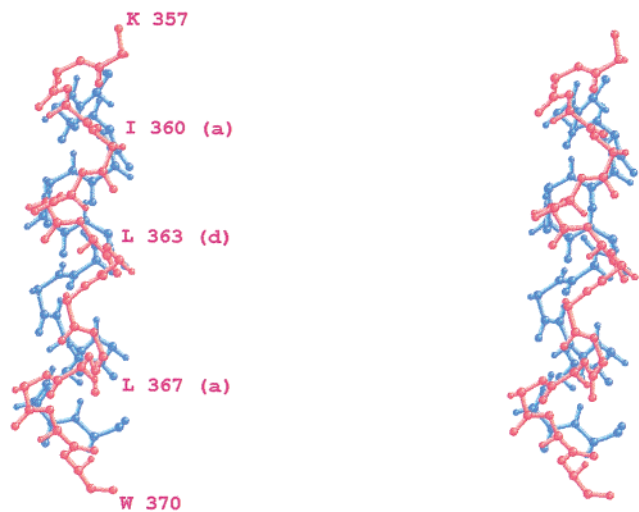

FIGURE 6: Stereoplot of a fit of the structures as seen in the XSA (blue) and calculated from NMR data (violet). For clarity, only the peptide backbone is displayed. Only the first part of the peptide is shown with Lys357 at the top and Trp370 at the bottom of the picture. The position of lipophilic amino acids in the a- and d-Positions crucial for coiled coil formation are marked for the NMR-structure.

distribution is rather wide with the exception of R369, A375, and D379. The first part of the peptide (up to W370) shows a helical motif, seen also in the crystal structure. A fit of this part of the calculated structure with the lowest target function and the corresponding sequence in the XSA using the peptide backbone as reference yields a RMSD value of 2.54 (Figure 6). When comparing the data originating from completely different systems in which the data sets were obtained (crystal vs solution) and the different length of the peptide/protein chains, the accordance of the structures with each other is quite good.

When compared over the whole sequence, the calculated structures display great diversity with high RMS values.

However, there are three regions within the peptide with pair wise similar structural motifs. The first is the N-terminal helix already mentioned (equivalent to the neck helix segment II of the X-ray structure). The match between the crystal and the solution structure is even better when only the amino acids V359−N368 are taken into account with an RMS of 2.35. Figure 7 displays 10 calculated structures fitted over the peptide backbone of amino acids V359−N368. The helical structure in the interval V359−N368 is readily seen. The next range with a defined structure is found between E374 and Q381 (Figure 8). Here, an extended region between E374 and V376 is followed by a bend from P377 to Q381. Finally, the residues I382 to K385 display a helical turn in the calculated structures (data not shown). The section R369 to G373 shows no structural preferences and can be considered a flexible region within the peptide as indicated in the wide distribution of the ϕ-angles for W370 and N372.

DISCUSSION

Most kinesin-like motors occur as dimers, with two ATP- and microtubule-binding domains (the "motor heads") linked via their coiled-coil rod domain. This has given rise to the idea that kinesin "walks" along the microtubule with both motor domains alternating (7, 8, 45). One consequence of the model is that each head must advance 16 nm at a time in order to achieve a center-of-mass step of 8 nm. When the X-ray structures of monomeric and dimeric kinesins became known (21, 23, 25, 27) they posed a problem because the heads are small, compared to the microtubule subunits, and they are tightly packed in the dimeric state (Figure 9). Therefore it seems impossible to move 8 nm, let alone 16 nm, unless the two heads splay apart temporarily during the movement. This can be done in several ways, by flipping the linker region and a partial opening of the coiled-coil connection between the heads (20, 36, 46). This makes the initial part of the rod domain of kinesin an important element in models of motility, rather than merely a passive connector between motor and cargo. In addition, kinesin shows a remarkable flexibility to adapt itself to different orientations of a microtubule, a property that was attributed to a flexible hinge near the head (32).

The rod of kinesin can be subdivided into several subdomains, a motor core domain, linker, neck, hinge, followed by a coiled-coil stalk and a tail (Figure 1). The dimeric kinesin construct solved by X-ray analysis extended to residue 379, but the polypeptide chain could only be identified up to the end of the neck helix (W370) while the rest was invisible, indicating either static disorder and/or flexibility. The present NMR structure of the peptide K357−D386 now yields an independent view of the neck domain, it extends the structure into the hinge region, and it identifies areas of rigidity and flexibility. One observes three structural motifs, a helix (K357−W370), extended chain with a bend (E374−Q381), and a turn (I382−D386), separated by flexible connections (at R371−G373 and Q381−I382). The initial helix agrees well with the X-ray structure (segment II of the neck helix, (37)). Figures 7 and 8 show two compound views of the NMR structure, centered on the initial helical stretch (Figure 7) or the extended chain stretch (Figure 8). In both cases it is remarkable how far the course of the peptide chain can diverge at the points of flexibility, up to the point of doubling back on itself. This situation becomes
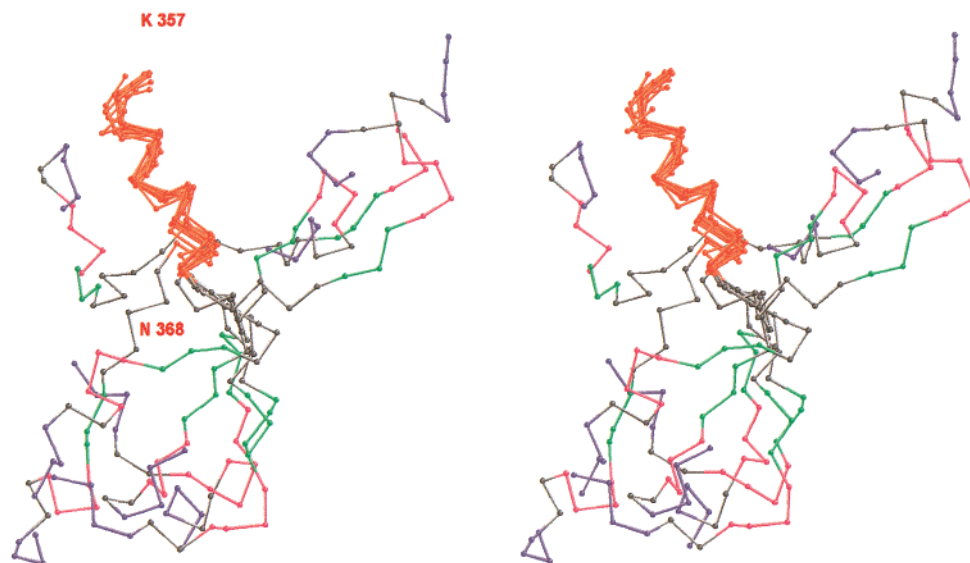
FIGURE 7: Stereoplot of 10 calculated structures superimposed in the α-helical region V359−N368 (K357 is at the top of the view). Only the α-carbon atoms are displayed. The structural motifs within the peptide are colored orange (helix, K357−N368), green (extended, E374−V376) purple (bend, P377−Q381), and blue (helical turn, I382−D386). The start and end of the helical interval are marked. In this superimposed view the course of the polypeptide chains diverges beyond the flexible area around N372.
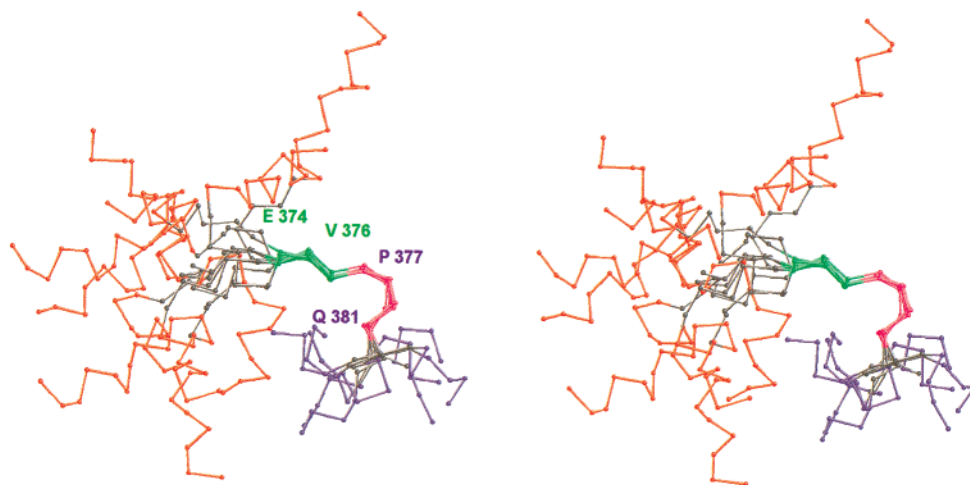

FIGURE 8: Stereoplot of 10 calculated structures fitted over the peptide backbone within the interval E374−Q381. The structural motifs within the peptide are colored orange (helix, K357−N368), green (extended, E374−V376), purple (bend, P377−Q381), and blue (helical turn, I382−D386). The C-terminal region is on the lower right. Only the α-carbon atoms are displayed. Both the start and the end of the extended region between E374 and V376 and of the turn between P377 and Q381 are marked. In this superposition the course of the peptide chain diverges beyond the two flexible points (∼372 in the left half, ∼381 in the right half of the figure)

even more apparent when superimposing the NMR structure on the full X-ray structure (Figure 9). The space swept out by the conformations of the hinge peptide becomes comparable with that of a motor domain. Since the peptide comprises only about half of the putative hinge region (∼370−410) before the next coiled-coil segment, it is likely that the conformational freedom of the hinge is even larger. If one takes this space as a measure of the flexibility of the hinge and if one assumes that the neck helix can splay apart during motility, it follows that the head domain could also acquire a highly mobile orientation−sufficient to adapt to the microtubule lattice during the initial attachment and during motion.

The effect of hinge flexibility has been probed in experiments where homologous hinges of kinesins from different sources were interchanged or replaced with α-helical, proline-rich, or other spacer sequences (33). The results showed that homologous exchanges with linkers from other kinesins left

the motility unchanged, but other spacer sequences could not substitute without affecting the speed, ATPase, and other parameters. Our results suggest a possible explanation: even though the hinge sequence appears "random" by prediction or spectroscopic methods, it contains well defined secondary structure motifs which are likely to be important for kinesin's function. Their exact role remains to be elucidated. Second, we believe that the points of flexibility are important for allowing the kinesin heads to probe their environment and to find new binding sites, as suggested by the biased diffusion model of motility (34). This would explain why general proline-rich sequences, which tend to be stiff (47), are not good substitutes for natural kinesin linkers.

Inspection of the neck helix of kinesin by prediction methods yields remarkable features. It can be subdivided into two segments on the basis of their internal structure (37). This corresponds to differences in folding and dimerization of peptides derived from the neck sequence (48−50) and to
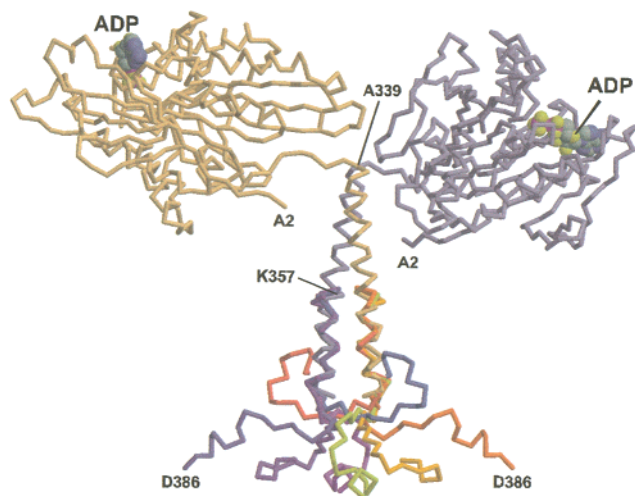
FIGURE 9: Superposition of X-ray structure of kinesin dimer [PDB code 3kin (*25*)] with a selected set of NMR solution structures (this study), aligned with respect to segment II of the neck helix (K357—W370). The X-ray structure (grey) shows the two motor domains (M, top) containing the microtubule-binding site and the nucleotide binding pocket (ADP shown in color). The coiled-coil neck helix (N) runs vertically, roughly in the plane of the paper. It is connected to the motor domain by an extended linker sequence (L). The X-ray and NMR structures agree well between K357 and W370. The X-ray density disappears beyond W370 due to disorder, whereas the NMR structures show many possible orientations.
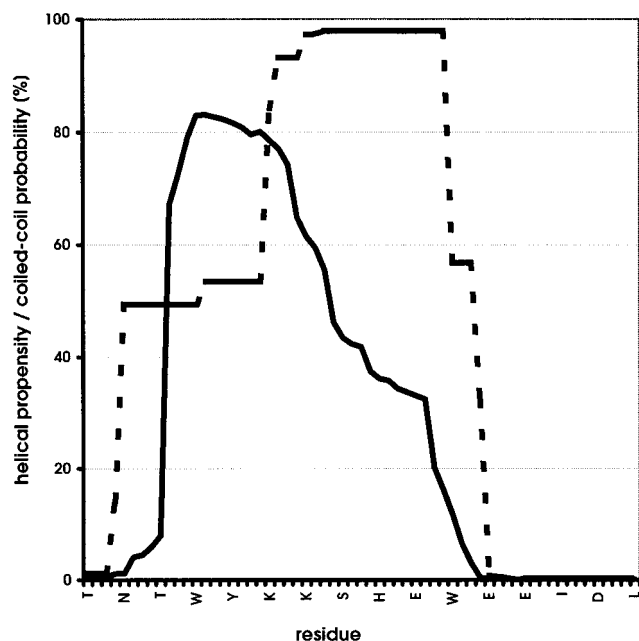

FIGURE 10: Predicted helix and coiled-coil propensities of the kinesin neck. Computations were done using the programs AGA-DIR (*51*) and COILS (*52*), using a window of 14 and 2.5-fold weighting of a and d positions. Note that segment I (A339—A355) has a high helix propensity but lower coiled-coil propensity, whereas segment II (L356—W370) shows the opposite effect. Experimentally, segment I alone is not sufficient to induce dimerization but acts cooperatively when segment II is present. Both segments are helical even in the monomeric form. For predictions see www.embl-heidelberg.de/Services/serrano/agadir/agadir-start.html and www.ch.embnet.org/software/COILS_form.html.

different predicted propensities for helix and coiled-coil formation (Figure 10). Segment I (V339—A355) has a high helix propensity [estimated by AGADIR (*51*)], and in agreement with this the helix of segment I is stable even in the monomeric state [as shown by the X-ray structure of

monomeric rK354 (*23*)]. However, this segment has a low coiled-coil propensity [estimated by COILS (*52*)] (*48*), due to an unusual cluster of charged residues and to charged or hydrophilic residues in the heptad positions a and d (e.g., E349, N354) which are antagonistic to coiled-coil formation. Similar nonstandard residues occur in transcription factors, e.g., GCN4 (*53, 54*), and in both cases they are thought to facilitate the opening-up of the coiled coil.

By contrast, segment II of the neck helix seen in the X-ray structure (L356—W370, corresponding to the N-terminal helix of the peptide determined by NMR) has a much lower predicted helix potential, yet a high coiled-coil potential because of the hydrophobic residues in a and d positions (corresponding to a leucine zipper). It was therefore not clear a priori whether segment II would still retain a helical conformation even in a monomeric form. We show here that this is indeed the case, possibly because of stabilizing intrachain salt bridges (H362—E366, heptad positions c—g, or E366—R369, heptad positions g—c). Another interesting feature of segment II is its potential role as a coiled-coil trigger sequence. These motifs, initially identified in cortexillin, help to nucleate the specific interaction between two α-helical domains in forming a coiled-coil (*55, 56*). The consensus sequence is LExchxcxccx (x = any residue, c = charged, h = hydrophobic) and closely agrees with the motif LEVELNRWRNG (residues 363—373). Trigger sequences are thought to operate through preferred interchain salt bridges, in the case of kinesin between E366 and R371 (g—e′ heptad positions). This postulated salt bridge has not been observed so far, since the helical order as well as rigidity is lost beyond W370 both in the monomeric and dimeric structure, and therefore the possible role of a coiled-coil nucleating trigger remains undecided for kinesin. We note however that the motif is highly conserved in conventional kinesins with N-terminal motor domains, suggesting an important function (*37*).

In summary, how do the results presented here bear on our understanding of kinesin motility? First, there is remarkable agreement between the X-ray and NMR results, emphasizing that the crystal structure is representative of the solution structure. Second, we have gained a partial view of the hinge domain that was formerly simply considered "disordered", but now shows local ordered motifs, separated by flexible joints, which can sweep out a large range of conformations and allow the heads to adopt many orientations. Third, both segments of the neck helix are stable enough to remain helical even when they are separated. This means that a hand-over-hand walking mechanism would require only the separation of the coiled-coil neck, but not the melting of the helices. Conversely, this would allow the coiled-coil to reform quickly, possibly with the help of the trigger sequence.

ACKNOWLEDGMENT

REFERENCES

1. Hirokawa, N. (1998) *Science 279*, 519—526.
2. Bloom, G. S., and Goldstein, L. S. B. (1998) *J. Cell Biol. 140*, 1277—1280.
3. Sheetz, M. P. (1999) *Eur. J. Biochem. 262*, 19—25.

4. Barton, N. R., and Goldstein, L. S. B. (1996) *Proc. Natl. Acad. Sci. U.S.A. 93*, 1735−1742.

5. Endow, S. A. (1999) *Eur. J. Biochem. 262*, 12−18.

6. Nogales, E., Whittaker, M., Milligan, R., and Downing, K. (1999) *Cell 96*, 79−88.

7. Howard, J. (1997) *Nature 389*, 561−567

8. Block, S. M. (1998) *J. Cell Biol. 140*, 1281−1284.

9. Cole, D. G., Scholey, J. M. (1995) *Trends Cell Biol. 5*, 259−262.

10. Brady, S. T., and Sperry, A. O. (1995) *Curr. Opin. Neurobiol. 5*, 551−558.

11. Stenoien, D., and Brady, S. T. (1997) *Mol. Biol. Cell. 8,* 675−689.

12. Tsai, M.-Y., Morfini, G., Szebenyi, G., and Brady, S. T. (2000) *Mol. Biol. Cell. 11,* 2161−2173.

13. Okada, Y., and Hirokawa, N. (2000) *Proc. Natl. Acad. Sci. U.S.A. 97*, 640−650.

14. Hackney, D. D. (1994) *Proc. Natl. Acad. Sci. U.S.A. 91*, 6865−6869.

15. Gilbert, S. P., Moyer, M. L., and Johnson, K. A. (1998) *Biochemistry 37*, 792−799.

16. Ma, Y. Z., and Taylor, E. (1997) *J. Biol. Chem. 272*, 724−730.

17. Berliner, E., Young, E. C., Anderson, K., Mahtani, H. K., and Gelles, J. (1995) *Nature 373*, 718−721.

18. Hancock, W., and Howard, J. (1998) *J. Cell Biol. 140*, 1395−1405.

19. Thormählen, M., Marx, A., Müller, S. A., Song, Y. H., Mandelkow, E. M., Aebi, U., and Mandelkow, E. (1998) *J. Mol. Biol. 275*, 795−809.

20. Hoenger, A., Sack, S., Thormählen, M., Marx, A., Müller, J., Gross, H., and Mandelkow, E. (1998) *J. Cell Biol. 141*, 419−430.

21. Kull, F. J., Sablin, E., Lau, P., Fletterick, R., and Vale, R. (1996) *Nature 380*, 550−554.

22. Sablin, E. P., Kull, F. J., Cooke, R., Vale, R. D., and Fletterick, R. J. (1996) *Nature 380*, 555−559.

23. Sack, S., Müller, J., Marx, A., Thormählen, M., Mandelkow, E.-M., Brady, S. T., and Mandelkow, E. (1997) *Biochemistry 36*, 16155−16165.

24. Gulick, A., Song, H., Endow, S., and Rayment, I. (1998) *Biochemistry 37*, 1769−1776.

25. Kozielski, F., Sack, S., Marx, A., Thormählen, M., Schönbrunn, E., Biou, V., Thompson, A., Mandelkow, E.-M., and Mandelkow, E. (1997) *Cell 91*, 985−994.

26. Sablin, E. P., Case, R. B., Dai, S. C., Hart, C. L., Ruby, A., Vale, R. D., and Fletterick, R. J. (1998) *Nature 395*, 813−816.

27. Sack, S., Kull, J., and Mandelkow, E. (1999) *Eur. J. Biochem. 262*, 1−11.

28. Sablin, E. (2000) *Curr. Opin. Cell Biol. 12*, 35−41.

29. Case, R. B., Pierce, D. W., Hom-Booher, N., Hart, C. L., and Vale, R. D. (1997) *Cell 90*, 959−966.

30. Henningsen, U., and Schliwa, M. (1997) *Nature 389*, 93−96.

31. Endow, S. A., and Waligora, K. W. (1998) *Science 281*, 1200−1202.

32. Hunt, A. J., and Howard, J. (1993) *Proc. Natl. Acad. Sci. U.S.A. 90*, 11653−11657.

33. Grummt, M., Woehlke, G., Henningsen, U., Fuchs, S., Schleicher, M., and Schliwa, M. (1998) *EMBO J. 17*, 5536−5542.

34. Mazumdar, M., and Cross, R. (1998) *J. Biol. Chem. 273*, 29352−29359.

35. Mandelkow, E., and Hoenger, A. (1999) *Cell Biol. 11*, 34−44.

36. Vale, R., and Milligan, R. A. (2000) *Science 288,* 88−95.

37. Thormählen, M., Marx, A., Sack, S., Mandelkow, E. (1998) *J. Struct. Biol. 122*, 30−41.

38. Braunschweiler, L., and Ernst, R. R. (1983) *J. Magn. Reson. 53*, 521−528.

39. Kumar, A., Wagner, G., Ernst, R. R., and Wüthrich, K. (1981) *J. Am. Chem. Soc. 103*, 3654−3658.

40. Eberstadt, M., Gemmecker, G., Mierke, D. F., and Kessler, H. (1995) *Angew. Chem. 107,* 1813−1838.

41. Neidig, K. P. (1996) in *Aurelia Software Manual*, Bruker GmbH, Karlsruhe.

42. Wüthrich, K. (1986) in *NMR of proteins and nucleic acids*, J. Wiley & Sons, New York.

43. Güntert, P., Mumenthaler, C., and Wüthrich, K. (1997) *J. Mol. Biol. 273*, 283−298.

44. Ludvigsen, S., Andersen, K. V., and Poulsen, F. M. (1991) *J. Mol. Biol. 217,* 731−736.

45. Mandelkow, E., and Johnson, K. A. (1998) *Trends Biochem. Sci. 23*, 429−433.

46. Romberg, L., Pierce, D., and Vale, R. (1998) *J. Cell Biol. 140*, 1407−1416.

47. Williamson, M. P. (1994) *Biochem. J. 297,* 249−260.

48. Tripet B., Vale, R. D., and Hodges, R. S. (1997) *J. Biol. Chem. 272*, 8946−8956.

49. Morii, H., Takenawa, T., Arisaka, F., and Shimizu, T. (1997) *Biochemistry 36*, 1933−1942.

50. Jiang, W., Stock, M. F., Li, X., and Hackney, D. D. (1997) *J. Biol. Chem. 272*, 7626−7632.

51. Munoz, V., and Serrano, L. (1994) *Nat. Struct. Biol. 1*, 399−409.

52. Lupas, A., Van Dyke, M., and Stock, J. (1991) *Science 252*, 1162−1164.

53. Alber, T. (1992) *Curr. Opin. Genet. Dev. 2*, 205−210.

54. Lupas, A. (1996) *Trends Biochem. Sci. 21*, 375−382

55. Steinmetz, M. O., Stock, A., Schulthess, T., Landwehr, R., Lustig, A., Faix, J., Gerisch. G, Aebi, U., and Kammerer, R. A. (1998) *EMBO J. 17*, 1883−1891.

56. Kammerer, R. A., Schulthess, T., Landwehr, R., Lustig, A., Engel, J., Aebi, U., and Steinmetz, M. O. (1998) *Proc. Natl. Acad. Sci. U.S.A. 95*, 13419−13424.